Measurement of Radical Quantum Yields from Formaldehyde Photolysis between 269 and 339 nm

Geoffrey D. Smith, Luisa T. Molina, and Mario J. Molina*

Department of Earth, Atmospheric and Planetary Sciences and Department of Chemistry, Massachusetts Institute of Technology, Cambridge, Massachusetts 02139

Received: August 16, 2001; In Final Form: November 5, 2001

The relative quantum yield for the production of radical products, H and HCO, from the photolysis of formaldehyde (HCHO) has been measured directly at wavelengths from 269 to 339 nm. Measurements of the radical products were conducted using chemical amplification with subsequent detection by chemical ionization mass spectrometry (CIMS). All yields were measured at a pressure of 50 Torr and were normalized to a quantum yield of 0.753 at 303.75 nm based on the recommendation of DeMore et al.[1] The quantum yields were measured with sufficient wavelength resolution (± 0.62 nm, fwhm) to observe structure which had been previously unreported and is believed to provide evidence for a complicated competition among the various dissociation pathways to H + HCO, H + H + CO and H_2 + CO, as well as with quenching to the ground state. The quantum yields measured should aid in the calculation of formaldehyde photolysis rates in the troposphere and are estimated to result in increases of at least 8% in calculated H/HCO production.

Introduction

The simplicity of the formaldehyde molecule has attracted much attention from spectroscopic,[2−6] photochemical,[7−11] and theoretical[12−14] investigations for many years. Increasingly sophisticated experiments have been designed and carried out leading to a more detailed and complete understanding of the molecule and its interaction with electromagnetic radiation. In recent years, the photodissociation of formaldehyde has also attracted attention due to its significant role as a source of radicals in the troposphere,[15] though it has been nearly twenty years since the last quantum yield measurements were published.

Formaldehyde is one of the most important carbonyl molecules in the lower atmosphere, being present in both polluted and rural areas. It is produced from the combustion of fossil fuels, the photochemical oxidation of methane and other hydrocarbons, as well as from biomass burning.[16,17]

The absorption of sunlight by formaldehyde can lead to dissociation via three pathways

$$\mathrm{HCHO} + h\nu \rightarrow \mathrm{H} + \mathrm{HCO} \qquad (\lambda \leq 330\ \mathrm{nm}) \qquad (1)$$

$$\rightarrow \mathrm{H_2} + \mathrm{CO} \qquad (\lambda \leq 361\ \mathrm{nm}) \qquad (2)$$

$$\rightarrow \mathrm{H} + \mathrm{H} + \mathrm{CO} \qquad (\lambda \leq 283\ \mathrm{nm}) \qquad (3)$$

where the wavelength limits represent the thermodynamic thresholds for each channel. The photolysis of formaldehyde to produce H_2 and CO (reaction 2) in the atmosphere constitutes a significant loss process for this molecule.

In addition, photodissociation via reaction 1 leads to the production of two radicals, H and HCO, both of which react in the presence of O_2 to create HO_2 radicals

$$\mathrm{H} + \mathrm{O_2} + \mathrm{M} \rightarrow \mathrm{HO_2} + \mathrm{M} \qquad (4)$$

$$\mathrm{HCO} + \mathrm{O_2} \rightarrow \mathrm{HO_2} + \mathrm{CO} \qquad (5)$$

The photolysis of larger aldehydes does not play as large of a role in the production of peroxy radicals as these molecules primarily absorb radiation at shorter wavelengths. Because the actinic flux reaching the troposphere is relatively weak at these wavelengths, the corresponding photolysis rates are smaller.

In polluted urban atmospheres (with high NO_x concentrations), reactions 1 and 3 do not represent a net loss of formaldehyde because the HO_2 radicals that are formed react in the presence of CH_4 and NO to ultimately regenerate formaldehyde. The creation of two HO_2 radicals per photon absorbed leads to a net increase in HO_x concentrations in the polluted troposphere. Additionally, convective injection of formaldehyde into the upper troposphere followed by photodissociation may serve as an additional source of HO_2 radicals in this region of the atmosphere. This mechanism could help to reconcile discrepancies between observed and modeled HO_x concentrations in the upper troposphere.[18,19]

The photolysis of formaldehyde has been shown to play a role in the formation of photochemical smog through the production of radical chain carriers (HO_2) which participate in the catalytic production of O_3[20,21]

$$\mathrm{HO_2} + \mathrm{NO} \rightarrow \mathrm{NO_2} + \mathrm{OH} \qquad (6)$$

$$\mathrm{NO_2} + h\nu \rightarrow \mathrm{O} + \mathrm{NO} \qquad (7)$$

$$\mathrm{O} + \mathrm{O_2} + \mathrm{M} \rightarrow \mathrm{O_3} + \mathrm{M} \qquad (8)$$

$$\mathrm{OH} + \mathrm{CO} \rightarrow \mathrm{CO_2} + \mathrm{H} \qquad (9)$$

$$\mathrm{H} + \mathrm{O_2} + \mathrm{M} \rightarrow \mathrm{HO_2} + \mathrm{M} \qquad (10)$$

$$\text{Net: } \mathrm{CO} + 2\,\mathrm{O_2} + h\nu \rightarrow \mathrm{CO_2} + \mathrm{O_3} \qquad (11)$$

In this catalytic chain, the HO_2 radical serves to convert NO to NO_2 (which leads to O_3 production), and in the presence of CO it is regenerated.

* To whom correspondence should be addressed.

10.1021/jp013180n CCC: $22.00
Published on Web 01/23/2002

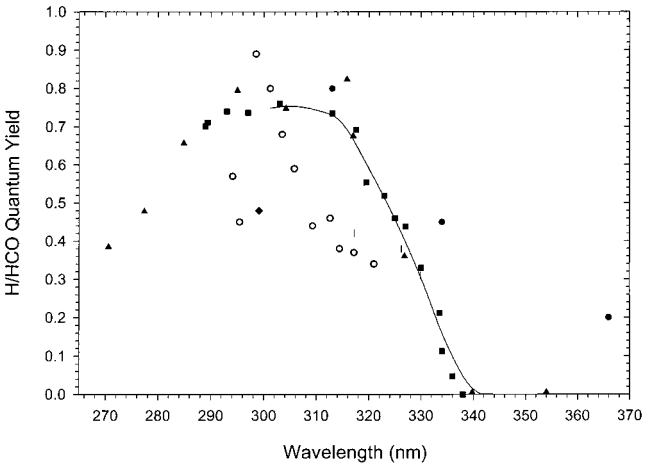

Figure 1. Previous radical (H + HCO) quantum yield measurement: Tang et al.[29] (○), Sperling & Toby[9] (●), Clark et al.[32] (◆), Horowitz & Calvert[28] (■), Moortgat et al.[31] (▲), and the recommendation of DeMore et al.[1] (—).

The need for accurate absorption spectra has continued to motivate high-resolution measurements of the formaldehyde cross section.[22−25] Likewise, the quantum yields for the radical channel (reaction 1) and the molecular channel (reaction 2) have been measured repeatedly in past years over a range of pressures and temperatures.[26−32] Nearly all of the studies of the radical channel quantum yield have been based on measurements of the H_2 and/or CO yields. In these experiments, the H radicals reacted with HCHO to produce H_2, or with a scavenger (such as isobutene) to generate other products. Estimations of the radical channel yield were then made either through comparison of the H_2 yields with and without the scavenger, or else through comparison with the CO yield. Similarly, Marling[33] measured radical yields from the photodissociation of deuterated formaldehyde by monitoring H_2, D_2, and HD.

Only one study[29] has measured the radical channel quantum yield through detection of a product unique to this channel. In that study, the chemiluminescence of HNO formed from the reaction of H and NO was monitored by Tang et al. The quantum yields obtained in this way are shown in Figure 1 along with those from other studies[9,28,31,32] in which the quantum yield was deduced from the yields of H_2 and/or CO. The yields of Tang et al. are significantly lower than those determined in the other studies precisely at those wavelengths at which formaldehyde absorbs light most efficiently and at which the solar flux increases rapidly.

Current recommendations[1,34] for the radical channel quantum yield are based primarily on the work of Horowitz and Calvert[28] and Moortgat et al.[31] (both detecting H_2 and/or CO yields). The agreement between these two sets of measurements is good, though some questions remain as to the reason for the discrepancy between these studies and that of Tang et al. In an effort to resolve this discrepancy, we have employed a broadband light source coupled to a monochromator for wavelength discrimination. Selective titration and chemical amplification of the H and HCO radical products were used, and subsequent detection and measurement of the yields was accomplished with chemical ionization mass spectrometry (CIMS). Use of the monochromator reduced the light flux available for photolysis but it offered continuous wavelength selection. The corresponding reduction in photolysis was compensated for by the high sensitivity of the CIMS detection technique.

Experiment

Monomeric formaldehyde was prepared from paraformaldehyde (Aldrich, 95% purity) using the procedure of Spence and Wild.[35] Formaldehyde was collected by condensing it in a cold trap in liquid N_2 (80 K) and then purified by warming in a trap in an 2-propanol/dry ice slush (196 K) and transferring to another trap in liquid N_2. Gas mixtures were then prepared by allowing the sample to warm and diluting a known pressure of the formaldehyde gas with N_2 (UHP Matheson). UV absorption spectroscopy and CIMS showed no evidence of any impurities. The NO used (UHP Matheson) was first purified by condensing any NO_2 impurity present in a finger held in an 2-propanol/dry ice slush. The purified NO was then diluted with N_2 to make the NO gas mixture.

A schematic diagram of the Photo-CIMS experimental apparatus is shown in Figure 2 and is described in detail in previous work.[36,37] A 75-Watt xenon arc lamp (Oriel 6137) produced white light that was focused into a monochromator (McKee-Pedersen Instruments 1018B) containing a diffraction grating (2360 lines mm^{-1}) used to disperse the light. The monochromator was calibrated over the entire range of wavelengths used in this study through the use of well-known Hg emission lines from a Hg pen lamp (UVP) to ensure accurate wavelength determination. The light flux exiting the photolysis tube was measured using a wavelength-calibrated photodiode (Oriel 70282).

The formaldehyde/N_2 flow (2−4 STP mL $min.^{-1}$), NO/N_2 flow (0.5 STP mL $min.^{-1}$) and O_2 (UHP Matheson) flow (2 STP mL $min.^{-1}$) were introduced and mixed at the rear of the photolysis tube. The photolysis tube was constructed of $^1/_4$ in. o.d. (4 mm i.d.) Pyrex tubing and was 11 cm in length. Residence times in the photolysis tube were on the order of one second, and the concentration of the formaldehyde in the photolysis tube was typically 1×10^{16} molecule cm^{-3}. The entire flow passed down the length of the tube and then entered the ion−molecule region where ionization was accomplished. A quadrupole mass spectrometer (ABB Extrel Merlin) was located at the end of the ion−molecule region. All gas flows were monitored with calibrated mass flow meters (Tylan). The pressures in the photolysis tube (∼50 Torr) and the ion−molecule region (∼25 Torr) were monitored using a 0−1000 Torr capacitance manometer (MKS Baratron).

Chemical ionization of the photolysis-titration products was achieved using the reagent ion, SF_6^-, which was generated by passing a 1500 STP mL min^{-1} flow of N_2 with SF_6 (∼1 ppm) through a ^{210}Po Nuclecel ionizer (NRD, Inc.). Ion−molecule gases (neutrals and ions) were drawn into the front chamber by a mechanical pump (Varian SD-450). The ions were focused by a 4 cm o.d. and 0.1 mm i.d. stainless steel plate held at −50 V and passed into a second chamber which contained the quadrupole mass filter pumped by a turbomolecular drag pump (Balzers TMU 520). A second turbomolecular drag pump pumped the rear chamber, which held the multiplier assembly. The same rotary pump (Varian SD-350) backed both turbomolecular drag pumps. The rear chamber was typically at a pressure of $\sim 10^{-5}$ Torr.

Measurement

Detection of Radicals and Chemical Amplification. The products of the radical dissociation channels, H and HCO, were not detected directly with chemical ionization. Instead, both

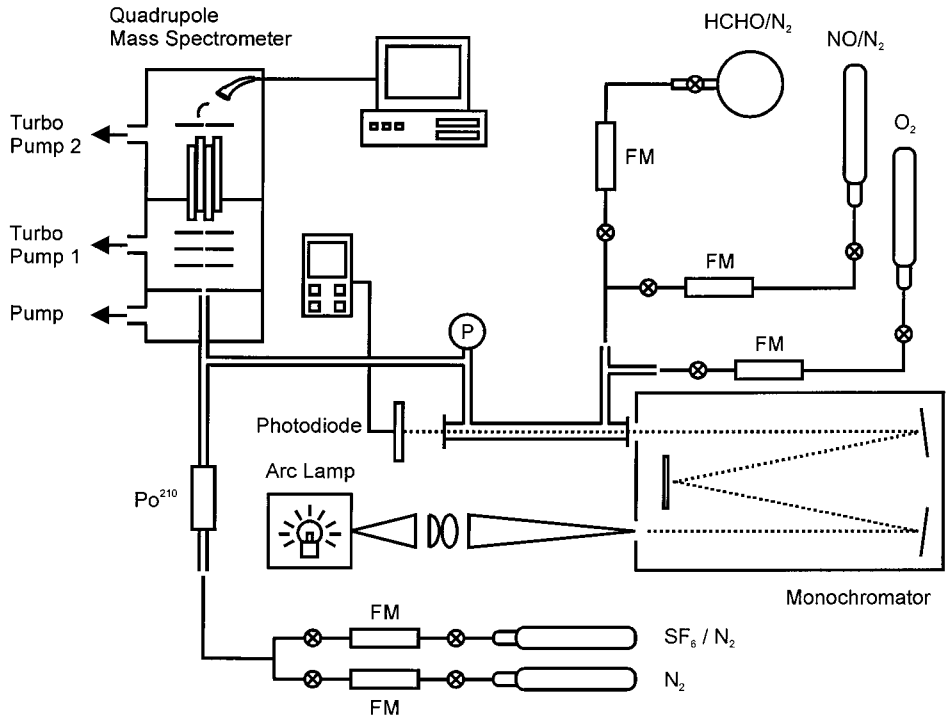

Figure 2. Schematic diagram of the Photo-CIMS system.

products were titrated with excess O_2 to convert them to HO_2 radicals

$$H + O_2 + M \rightarrow HO_2 + M \quad (4)$$

$$HCO + O_2 \rightarrow HO_2 + CO \quad (5)$$

The reactions of HO_2 with itself limited the ability to measure HO_2 directly

$$HO_2 + HO_2 \rightarrow H_2O_2 + O_2 \quad (12)$$

Reaction with the large concentration of formaldehyde present could also remove HO_2

$$HO_2 + HCHO + M \rightarrow HOCH_2OO + M \quad (13)$$

However, the adduct formed is not thermally stable and therefore reaction 13 will not result in net removal of HO_2. Additionally, the small absorption cross section of formaldehyde at these wavelengths (the maximum cross section is $\sim 9 \times 10^{-20}$ cm^2 molecule^{-1} near 304 nm[23]) and the low light flux available from the arc lamp resulted in very small concentrations of the photoproducts.

In an effort to enhance detection of these photoproducts, a chemical amplification scheme based on the peroxy radical measurements of Cantrell et al.[37,38] was implemented. In this scheme the HO_2 radicals reacted with excess NO to produce NO_2

$$HO_2 + NO \rightarrow NO_2 + OH \quad (6)$$

The NO_2^- was easily detected with CIMS

$$NO_2 + SF_6^- \rightarrow NO_2^- + SF_6 \quad (14)$$

In addition to converting HO_2 to NO_2, reaction 6 leads to the production of an OH radical. The OH radical reacts quickly with the large concentration of formaldehyde that is present to regenerate the HCO radical

$$OH + HCHO \rightarrow HCO + H_2O \quad (15)$$

and this reaction completes the chemical amplification of the photoproducts

$$H + O_2 + M \rightarrow HO_2 + M \quad (4)$$

$$HCO + O_2 \rightarrow HO_2 + CO \quad (5)$$

$$HO_2 + NO \rightarrow NO_2 + OH \quad (6)$$

$$OH + HCHO \rightarrow HCO + H_2O \quad (15)$$

$$\text{Net: } HCHO + NO + O_2 \rightarrow NO_2 + H_2O + CO \quad (16)$$

In this way, the slow rate of photodissociation was enhanced through the amplification of the yields of the radical photoproducts.

Linearity of Chemical Amplification. Measurement of radical quantum yields through the detection of NO_2 required that the chemical amplification be linear with the rate of production of H and HCO radicals. Tests were therefore performed in which the NO_2^- signal rise from the photolysis and subsequent chemical amplification was monitored as a function of the light flux in the photolysis tube (Figure 3). With the introduction of a variable neutral density filter at the entrance to the monochromator, the flux in the photolysis tube was adjusted while all of the other parameters such as wavelength and bandwidth of the light and concentrations and flows of the gases were held constant. It was found that the scheme amplified the radical signal by a factor of about 35 and that the signal rise was linear over a range of more than 50 in the light flux. These findings further indicated that the signal could be expected to remain linear over a correspondingly wide range of values of the absorption cross section and quantum yield. In practice, relative measurements were made by matching the rate of

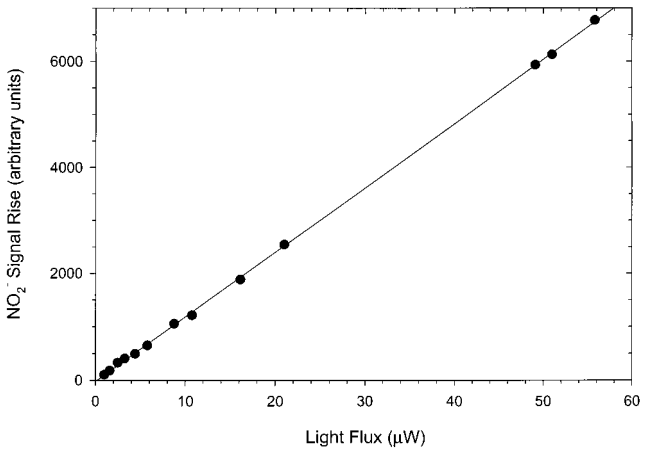

Figure 3. Experiment performed to determine response of chemical amplification with light flux ($\lambda = 304.6$ nm). Line represents a least-squares fit to the data.

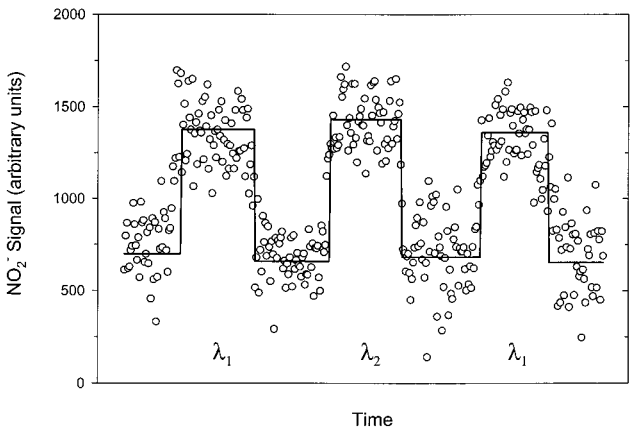

Figure 4. Sample signal rises with wavelength alternated between reference ($\lambda_1 = 303.75$ nm) and measurement ($\lambda_2 = 328.75$ nm). Light flux at λ_1 is attenuated by approximately 70% in order to match the signal rise at the two wavelengths.

photodissociation to that at a reference wavelength, so that linearity over such a large range was not required. The linearity in the NO_2^- signal observed in these tests thus confirmed that the chemical amplification scheme could be used in making the quantum yield measurements. This linearity also indicated that the chain amplification is terminated by a first-order reaction, which might be a reaction at the wall or a pseudo-first-order reaction with a species present in large concentration (such as O_2 or HCHO). Finally, the kinetics of the chemical amplification scheme were modeled using published values for the rate coefficients for all of the reactions expected to be present in the experiments. Though the modeling confirmed that the amplification was linear under the conditions of the experiment, the calculated amplification chain length was found to be approximately 135, nearly four times larger than was measured. We believe that this disparity reflects the omission of a first-order chain termination mechanism in the model, such as a wall reaction or a neglected gas-phase reaction, for example $HCO + O_2 + M \rightarrow HCO_3 + M$.

Relative Quantum Yields. Relative quantum yield measurements were made by comparison of NO_2^- yields at various wavelengths relative to the yield at a reference wavelength of 303.75 nm. This reference wavelength was chosen for the following reasons. First, the formaldehyde absorption cross section at this wavelength is relatively large (4.33×10^{-20} cm^2).[23] Second, the H/HCO quantum yield is believed to be fairly large (0.753) and constant around this wavelength.[1] All relative measurements were placed on an absolute scale by normalizing to a value of 0.753 at this wavelength.

The wavelength of the light in the photolysis tube was alternated between the reference and measurement wavelengths (see Figure 4) by changing the angle of the diffraction grating in the monochromator. Measurements were typically made using an exposure time of three minutes at each wavelength. Only the photolysis wavelength was changed, while other variables (including gas flows and concentrations) were kept constant between successive measurements. However, if the effective rates of photolysis at the reference and measurement wavelengths were significantly different, then secondary reactions involving species produced in the titration (such as HO_2 and NO_2) would be different, as well.

To minimize the effects of this secondary chemistry on the species being measured, the NO_2 concentration (as measured by the NO_2^- signal) was matched at the two wavelengths. Placement of a variable neutral density filter at the entrance slit of the monochromator allowed the light to be attenuated and the magnitude of the NO_2^- signal to be controlled. With comparable concentrations of all trace species at the two wavelengths, similar detection sensitivities and secondary chemistry were ensured. This procedure allowed a direct comparison of the photolysis-titration product yields obtained at the measurement and reference wavelengths.

Calculation of Quantum Yields. The absolute quantum yield at the measurement wavelength (λ_2) was calculated relative to that at the reference wavelength (λ_1) through use of the following expression (derived in previous work[36,37])

$$\phi_{\lambda_2} = \phi_{\lambda_1} \frac{S_{\lambda_2}}{S_{\lambda_1}} \frac{I_{\lambda_1}}{I_{\lambda_2}} \frac{\lambda_1}{\lambda_2} \frac{[\exp(\sigma_{\lambda_1}[\mathrm{HCHO}]l) - 1]}{[\exp(\sigma_{\lambda_2}[\mathrm{HCHO}]l) - 1]} \qquad (17)$$

In this expression, S_λ is the NO_2^- signal rise, and I_λ is the light flux (in Watts). Values for σ_λ represent the formaldehyde absorption cross section (high-resolution cross section data from Cantrell et al.[23]) weighted by the known monochromator shape function over the given bandwidth (usually ± 0.625 nm, fwhm). The highly structured absorption by formaldehyde demanded careful consideration of the effect of the shape function (triangular in this case) on the distribution of the light entering the photolysis tube in order to accurately determine the quantum yields.

The effect of the monochromator shape function on the effective absorption spectrum of formaldehyde is shown in Figure 5. Here, the shape function (shown in the inset) results in less light exiting the monochromator at the edges of the bandwidth, and the peak in cross section near 329.5 nm is somewhat attenuated. This effect results in a very different value for the average cross section over this bandwidth. In fact, in this example, the weighted cross section is approximately 20% smaller than the simple average cross section. This difference, if not accounted for, would result in a corresponding error of 20% in the calculation of the quantum yield.

Besides affecting the magnitude of the average cross section, the highly structured features in the absorption spectrum lead to asymmetric weighting. In some cases, the majority of the absorption over a given bandwidth results from an intense peak near the edge of the bandwidth. The quantum yield that is measured is then more representative of this wavelength than of the "central" wavelength. In the example shown in Figure 5, the central wavelength is shifted from 328.75 to 329.16 nm due to the peak near 329.5 nm.

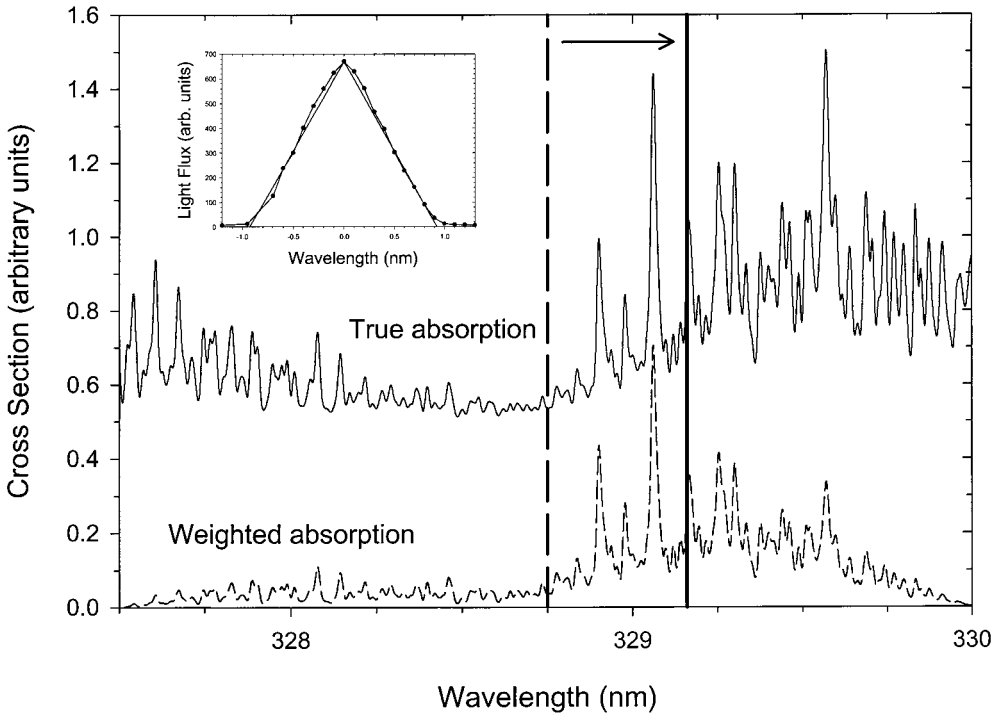

Figure 5. Effect of the triangular shape function of the monochromator (shown in the inset) on the absorption spectrum of formaldehyde (—) resulting in a weighted spectrum (− −). The shift in the vertical lines represents the shift in the midpoint or the wavelength at which the weighted absorption is divided into equal areas on either side. The weighting reduces the average cross section by 20% and would result in a corresponding error in the measurement of the quantum yield if not taken into account. Note that the true absorption has been shifted upward for clarity. (Cross section data from Cantrell et al.[23])

In addition to weighting the high-resolution absorption cross section data of Cantrell et al.[23] with the monochromator shape function, direct measurements of the formaldehyde absorption were carried out. Light from the arc lamp was filtered by the monochromator, just as in the quantum yield measurements, and the light flux was measured at the end of the photolysis tube with the photodiode. The light flux was measured both with and without the formaldehyde present, and from these absorptions effective cross sections were determined. The quantum yields were then calculated using these cross sections and a simplified form of eq 17

$$\phi_{\lambda_2} = \phi_{\lambda_1} \frac{S_{\lambda_2}}{S_{\lambda_1}} \frac{I_{\lambda_1}}{I_{\lambda_2}} \frac{\lambda_1}{\lambda_2} \frac{\sigma_{\lambda_1}}{\sigma_{\lambda_2}} \tag{18}$$

This equation is obtained by replacing the exponential terms in eq 17 with a Taylor expansion, with the second-order and higher terms neglected. With maximum values for σ_λ of 9×10^{-20} cm^2 molecule^{-1}, [HCHO] $\sim 10^{16}$ molecules cm^{-3} and $l = 11$ cm, the exponent is never larger than 0.01, and the omission of the higher-order terms in the Taylor expansion results in a negligible error for all measurements made.

The absorption measurements were conducted relative to those at the reference wavelength (303.75 nm). This procedure eliminated the need for the absolute determination of the formaldehyde concentration (as required, in principle, by the use of eq 17). In addition, the absorption measurements made in this manner automatically reflect the weighting by the monochromator shape function since they were made with the same bandwidths as in the quantum yield measurements. Finally, these measurements diminished the potential effect that stray light of unwanted wavelengths which may have exited the monochromator could have on the quantum yield experiments. The measurements include absorption of any stray light that might be present in addition to absorption of the light of the selected wavelengths. This method of measuring the weighted cross sections thus factored out any possible absorption of stray light in the calculation of the quantum yields.

The effective absorption cross sections determined both through the direct measurement of the absorptions as well as through the weighting of the cross section data of Cantrell et al. are shown in Table 1. The effective wavelengths listed, λ_{eff}, represent the shifts in the "central" wavelengths calculated from the asymmetry in the absorption over each bandwidth. The two methods can be seen to compare favorably at nearly all wavelengths and bandwidths used. The lack of any systematic offset to larger or smaller values indicates that there is little systematic error present in the absorption measurements. In addition, the general agreement between the two methods indicates that the presence of stray light in the monochromator is minimal and does not affect the quantum yield measurements.

The notable exception to the good agreement, at 333.75 nm, results most likely from difficulties in measuring the very small cross section at high resolution at that wavelength. The wide bandwidth of the monochromator measurements probably results in smaller errors since these measurements represent integrated absorptions over the entire bandwidth. Therefore, all quantum yields listed in Table 1 were calculated with the absorption data measured in this work with the monochromator. These quantum yields are shown in Figure 6 along with the data of Horowitz & Calvert,[28] Tang et al.,[29] Moortgat et al.,[31] as well as the recommendation of DeMore et al.[1] for comparison. The errors quoted represent 95% confidence limits and include estimated uncertainties in both the measurements of the NO_2^- yields as well as the absorption measurements; however they do not reflect the uncertainty in the quantum yield at the reference wavelength of 303.75 nm. It should be noted that the uncertainty

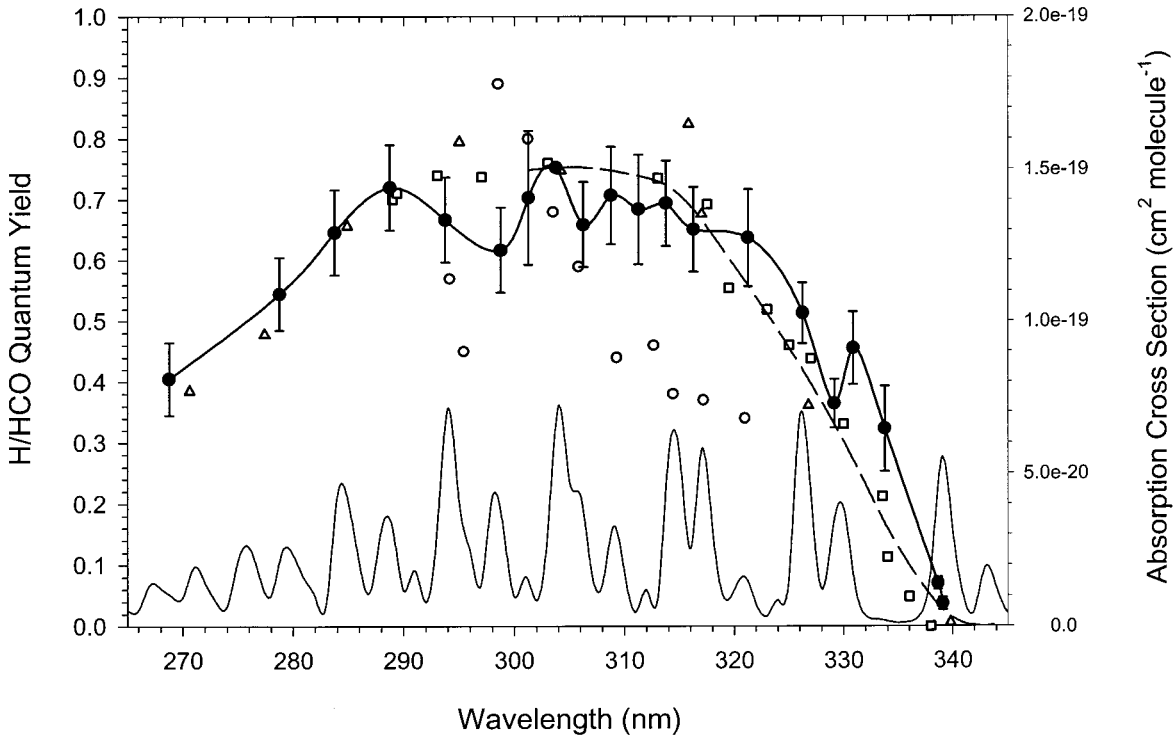

Figure 6. Radical (H/HCO) quantum yields. This work (●), Horowitz & Calvert[28] (□), Tang et al.[29] (○), Moortgat et al.[31] (△), and recommendation of DeMore et al.[1] (− −). The absorption spectrum[25] is shown at the bottom for reference. Error bars on the quantum yield data represent 95% confidence limits.

TABLE 1: Radical (H/HCO) Quantum Yields Measured in This Work

λ (nm)	λ_{eff}[a] (nm)	$\Delta\lambda$[b] (nm)	σ_{rel} (meas)[c]	σ_{rel} (calc)[d]	ϕ[e]
268.75		± 0.62	0.151		0.41 ± 0.06
278.75		± 0.62	0.269		0.55 ± 0.06
283.75		± 0.62	0.442		0.65 ± 0.07
288.75		± 0.62	0.506		0.72 ± 0.07
293.75		± 0.62	0.995		0.67 ± 0.07
298.75		± 0.62	0.576		0.62 ± 0.07
301.25		± 0.62	0.238		0.70 ± 0.11
303.75			1	1	0.753[f]
306.25	306.09	± 0.62	0.580	0.640	0.66 ± 0.07
308.75	308.86	± 0.62	0.495	0.480	0.71 ± 0.08
311.25	311.28	± 0.62	0.103	0.135	0.68 ± 0.09
313.75	314.13	± 0.62	0.592	0.605	0.69 ± 0.07
316.25	316.42	± 0.62	0.576	0.603	0.65 ± 0.07
321.25	321.13	± 0.62	0.209	0.226	0.64 ± 0.08
326.25	326.08	± 0.62	0.967	1.029	0.51 ± 0.05
328.75	329.16	± 0.62	0.311	0.355	0.36 ± 0.04
331.25	330.87	± 0.62	0.180	0.199	0.46 ± 0.06
333.75	333.24	± 1.25	0.061	0.029	0.30 ± 0.07
336.25	338.65	± 1.80	0.215	0.202	0.07 ± 0.01
338.75	339.09	± 1.80	0.546	0.597	0.04 ± 0.01

[a] The effective wavelength represents the asymmetry of the absorption cross section over the bandwidth employed. [b] Full-width at half-maximum. [c] Absorption cross section measured relative to that at 303.75 nm. [d] Absorption cross section calculated with the known shape function of the monochromator and the cross section data of Cantrell et al.[23] [e] Quoted errors represent 95 % confidence limits and include uncertainties in σ_{rel} (meas). [f] Normalization wavelength, $\phi = 0.753$ taken from DeMore et al.[1]

in the cross section constitutes a large fraction of the error in the quantum yield at most wavelengths.

Discussion

Dissociation Dynamics. The quantum yields for H and HCO production measured in this study show structure which had been previously unreported. These results provide a new confirmation of the complexity associated with the photodissociation of formaldehyde at wavelengths in the UV.

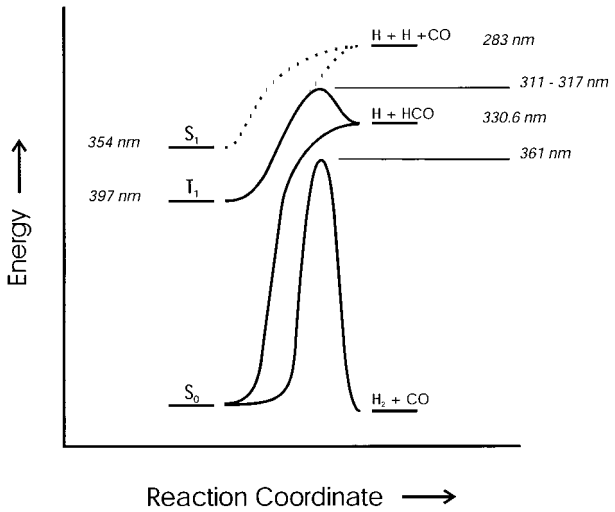

Figure 7. Energy level diagram for relevant excited states of formaldehyde with correlated dissociation channels (adapted from Houston & Moore[3]). Wavelength thresholds taken from: Hayes & Morokuma,[12] Chuang et al.,[5] Polik et al.,[42] and Bruna et al.[14]

The absorption of light by formaldehyde occurs through the electronic excitation from the ground singlet state of the molecule (S_0) to the first excited singlet state (S_1), with some excitation from the ground state to the first excited triplet state (T_1).[2,3,5,8,13,40] Many challenging experiments and theoretical studies have investigated the processes controlling the redistribution of energy within the molecule. Even without extensive knowledge of the potential energy surfaces involved, the roles of these processes have been clarified, and these are summarized in Figure 7. The wavelengths shown in the figure represent the appropriate energetic thresholds.

Upon excitation to S_1, a few pathways are possible: 1) internal conversion to highly vibrationally excited states of S_0, 2) quenching to lower energy (bound) states of S_0, 3) "spin-forbidden" transition to vibrationally excited states of T_1, and 4) (conjectured) direct dissociation via reaction 3 (H + H + CO). The highly vibrationally excited states of S_0 can lead to dissociation via reaction 1 (H + HCO) as well as via reaction 2 (H_2 + CO). The vibrationally excited states of T_1 lead to dissociation to H + HCO or perhaps to H + H + CO.

The barriers evident for dissociation from T_1 to H + HCO and from S_0 to H_2 + CO result in calculated threshold wavelengths[5,12,14,42] (311−317 and 361 nm, respectively) shorter than the thermodynamic thresholds of the corresponding products. Competition between these various dissociation pathways as well as quenching processes leads to complicated energy distribution following absorption of light at wavelengths in the UV. The radical quantum yields here represent the first measurements to confirm this complicated behavior in the dissociation to radical products. Previous measurements of the radical quantum yields[28,31,32] appear much smoother and lack the structure that is apparent in the measurements presented here. The quantum yields reported by Tang et al.[29] do show a distinct peak near 300 nm, but the limited range of wavelengths employed precludes a more complete interpretation in terms of the many competing dissociation pathways.

Absorption by vibrationally excited molecules in the ground electronic state can extend the wavelength threshold for dissociation via a particular channel past its thermodynamic threshold. Excitation of one quantum in the lowest vibrational mode (∼1200 cm^{-1} [13,41,42]) is calculated to extend the threshold for dissociation via reaction 1 as much as about 8 nm past the thermodynamic threshold of 330 nm. Likewise, the observed threshold for dissociation from T_1 to H + HCO via the barrier could be extended by about 8 nm past the calculated threshold ranging from 311 nm to 317 nm. The threshold wavelength for dissociation to H + H + CO could also be extended from 283 nm to approximately 291 nm.

The shift to longer wavelength of the thresholds for dissociation via the various channels could explain the location of the structure in the radical quantum yields measured with the Photo-CIMS system. The peak near 289 nm may correspond to the onset of reaction 3 (H + H + CO) just as the peak near 330 nm may correspond to the onset of reaction 1 (H + HCO) via dissociation from the S_0 state. The apparent peak near 304 nm is more difficult to interpret and may be due to a complicated interaction between internal conversion to S_0 and intersystem crossing to T_1. Nonetheless, the structure observed in the radical quantum yield measurements reported here supports theories proposing that dissociation proceeds through a complicated competition among the various pathways.

Finally, the radical yields measured at short wavelengths ($\lambda \leq 290$ nm) could very well be due to dissociation via reaction 3 (H + H + CO) and not via reaction 1 (H + HCO). The large concentration of O_2 required in these experiments results in conversion of both H and HCO radicals to HO_2, and it is therefore not possible to distinguish between these two dissociation channels. However, photons in this region of the spectrum possess enough energy to lead to dissociation via reaction 3, especially when absorption by vibrationally excited formaldehyde molecules is considered.

Thus, the quantum yield measurements appear to support dissociation via three different routes: (1) from excited S_0, (2) from excited T_1 and over a barrier, and (3) directly from the initial excited state, S_1.

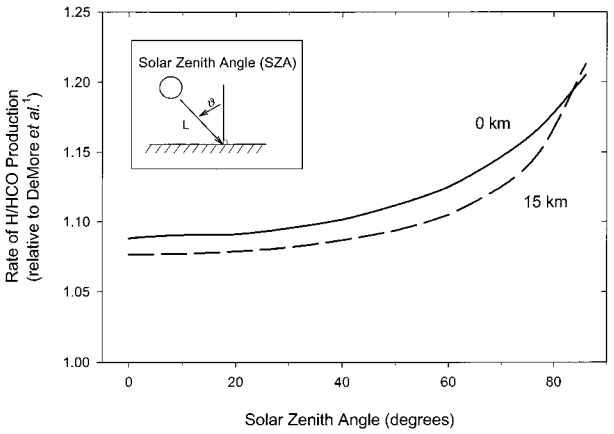

Figure 8. Increase in HO_2 production rate at 0 km (—) and at 15 km (− −) calculated using the quantum yield data from this work relative to the recommendation by DeMore et al.[1]

Atmospheric Implications. The quantum yields for the production of H and HCO radicals from the photolysis of formaldehyde as measured in this work agree qualitatively with the yields reported by Horowitz & Calvert[28] and Moortgat et al.,[31] as well as with the recommendation of DeMore et al.[1] (Figure 6). The rapid rise in solar flux in the troposphere at wavelengths longer than 300 nm, however, amplifies the small differences in the quantum yield values, and this results in a noticeable change in the calculated photodissociation rate of formaldehyde in the troposphere.

The net effect on the radical production from the photolysis of formaldehyde in the atmosphere can be represented as a change in the calculated rate of production of radical photoproducts. In Figure 8, the rate of production relative to that calculated using the recommendation of DeMore et al.[1] is shown as a function of solar zenith angle. The net increase ranges from 8% to 21% with the largest effect at the larger zenith angles where the solar flux reaching the earth is enriched in longer-wavelength ($\lambda > 320$ nm) radiation. At these wavelengths, the quantum yields measured in this work are larger than those recommended[1] and result in a larger rate of radical production. It is important to emphasize that the sole factor leading to the enhancement in the radical yield is the difference between our measured quantum yields and those recommended by DeMore et al.[1] at $\lambda > 320$ nm.

Conclusion

The work presented here represents only the second study in which radical products from the photolysis of formaldehyde have been measured directly and independently of the molecular products. The successful use of chemical amplification of the radical products has allowed the measurement of these quantum yields over a range of wavelengths in the UV with sufficient resolution to observe structure that had not been reported previously. The quantum yield values reported in this work differ from the values recommended by DeMore et al.[1] especially at longer wavelengths ($\lambda > 320$ nm) at which the actinic flux increases rapidly. The net calculated H/HCO production from photolysis of formaldehyde in the troposphere is estimated to increase by at least 8% by using the quantum yields measured in this work.

Acknowledgment. This research was supported by a grant from the National Aeronautics and Space Administration

Upper Atmosphere Research Program. We thank Chris Cantrell and Jack Calvert for providing high-resolution formaldehyde absorption cross section data. G.D.S. acknowledges support from the National Science Foundation Environmental Chemistry Traineeship.

References and Notes

(1) DeMore, W. B.; Sander, S. P.; Howard, C. J.; Ravishankara, A. R.; Golden, D. M.; Kolb, C. E.; Hampson, R. F.; Kurylo, M. J.; Molina, M. J. NASA Panel for Data Evaluation, Chemical Kinetics and Photochemical Data for Use in Stratospheric Modeling, JPL Publication 97-4, 1997.

(2) Yeung, E. S.; Moore, C. B. *J. Chem. Phys.* **1973**, *58*, 3988.

(3) Houston, P. L.; Moore, C. B. *J. Chem. Phys.* **1976**, *65*, 757.

(4) Shibuya, K.; Harger, R. A.; Lee, E. K. C. *J. Chem. Phys.* **1978**, *69*, 751.

(5) Chuang, M.-C.; Foltz, M. F.; Moore, C. B. *J. Chem. Phys.* **1987**, *87*, 3855.

(6) Terentis, A. C.; Kable, S. H. *Chem. Phys. Lett.* **1996**, *258*, 626.

(7) Klein, R.; Schoen, L. J. *J. Chem. Phys.* **1956**, *24*, 1094.

(8) Abrahamson, E. W.; Littler, J. G. F.; Vo, K.-P. *J. Chem. Phys.* **1966**, *44*, 4082.

(9) Sperling, H. P.; Toby, S. *Can. J. Chem.* **1973**, *51*, 471.

(10) Lewis, R. S.; Tang, K. Y.; Lee, E. K. C. *J. Chem. Phys.* **1976**, *65*, 2910.

(11) Lewis, R. S.; Lee, E. K. C. *J. Phys. Chem.* **1978**, *82*, 249.

(12) Hayes, D. M.; Morokuma, K. *Chem. Phys. Lett.* **1972**, *12*, 539.

(13) Scuseria, G. M.; Schaefer, H. F., III *J. Chem. Phys.* **1989**, *90*, 3629.

(14) Bruna, P. J.; Hachey, M. R. J.; Grein, F. *J. Mol. Struct. (THEOCHEM)* **1997**, *400*, 177.

(15) Calvert, J. G.; Kerr, J. A.; Demerjian, K. L.; McQuigg, R. D. *Science* **1972**, *175*, 751.

(16) Carlier, P.; Hannachi, H.; Mouvier, G. *Atm. Environ.* **1986**, *20*, 2079.

(17) Anderson, L. G.; Lanning, J. A.; Barrell, R.; Miyagishima, J.; Jones, R. H.; Wolfe, P. *Atm. Environ.* **1996**, *30*, 2113.

(18) Jaeglé, L.; Jacob, D. J.; Brune, W. H.; Tan, D.; Faloona, I. C.; Weinheimer, A. J.; Ridley, B. A.; Campos, T. L.; Sachse, G. W. *Geo. Res. Lett.* **1998**, *25*, 1709.

(19) Prather, M. J.; Jacob, D. J. *Geo. Res. Lett.* **1997**, *24*, 3189.

(20) Wayne, R. P. *Chemistry of Atmospheres*; Oxford University Press: Oxford, 1994; pp 91−94.

(21) Finlayson-Pitts, B. J.; Pitts, J. N., Jr. *Chemistry of the Upper and Lower Atmosphere*; Academic Press: San Diego, 2000; pp 89, 93.

(22) Bass, A. M.; Glasgow, L. C.; Miller, C.; Jesson, J. P.; Filkin, D. L. *Planet. Space Sci.* **1980**, *28*, 675.

(23) Cantrell, C. A.; Davidson, J. A.; McDaniel, A. H.; Shetter, R. E.; Calvert, J. G. *J. Phys. Chem.* **1990**, *94*, 3902.

(24) Rogers, J. D. *J. Phys. Chem.* **1990**, *94*, 4011.

(25) Meller, R.; Moortgat, G. K. *J. Geo. Res.* **2000**, *105*, 7089.

(26) DeGraff, B. A.; Calvert, J. G. *J. Am. Chem. Soc.* **1967**, *89*, 2247.

(27) McQuigg, R. D.; Calvert, J. G. *J. Am. Chem. Soc.* **1969**, *91*, 1590.

(28) Horowitz, A.; Calvert, J. G. *Int. J. Chem. Kinet.* **1978**, *10*, 805.

(29) Tang, K. Y.; Fairchild, P. W.; Lee, E. K. C. *J. Phys. Chem.* **1979**, *83*, 569.

(30) Moortgat, G. K.; Warneck, P. *J. Chem. Phys.* **1979**, *70*, 3639.

(31) Moortgat, G. K.; Seiler, W.; Warneck, P. *J. Chem. Phys.* **1983**, *78*, 1185.

(32) Clark, J. H.; Moore, C. B.; Nogar, N. S. *J. Chem. Phys.* **1978**, *68*, 1264.

(33) Marling, J. *J. Chem. Phys.* **1977**, *66*, 4200.

(34) Atkinson, R.; Baulch, D. L.; Cox, R. A.; Hampson, R. F., Jr.; Kerr, J. A.; Rossi, M. J.; Troe, J. *J. Phys. Chem. Ref. Data* **1997**, *26*, 521.

(35) Spence, R.; Wild, W. *J. Chem. Soc.* **1935**, 338.

(36) Smith, G. D.; Molina, L. T.; Molina, M. J. *J. Phys. Chem. A* **2000**, *104*, 8916.

(37) Smith, G. D.; Tablas, F.; Molina, L. T.; Molina, M. J. *J. Phys. Chem. A* **2001**, *105*, 8658.

(38) Cantrell, C. A.; Stedman, D. H.; Wendel, G. J. *Anal. Chem.* **1984**, *56*, 1496.

(39) Cantrell, C. A.; Shetter, R. E.; Lind, J. A.; McDaniel, A. H.; Calvert, J. G.; Parrish, D. P.; Fehsenfeld, F. C.; Buhr, M. P.; Trainer, M. *J. Geo. Res.* **1993**, *98*, 2897.

(40) Ho, P.; Bamford, D. J.; Buss, R. J.; Lee, Y. T.; Moore, C. B. *J. Chem. Phys.* **1982**, *76*, 3631.

(41) Reisner, D. E.; Field, R. W.; Kinsey, J. L.; Dai, H.-L. *J. Chem. Phys.* **1984**, *80*, 5968.

(42) Polik, W. F.; Guyer, D. R.; Moore, C. B. *J. Chem. Phys.* **1990**, *92*, 3453.